PERGAMON

International Journal of Multiphase Flow 26 (2000) 741–761

International Journal of Multiphase Flow

www.elsevier.com/locate/ijmulflow

Droplet transport in oil/gas and water/gas flow at high gas densities

D. Tayebi[a,*], S. Nuland[b], P. Fuchs[c]

[a]*Department of Mathematics, University of Oslo, Oslo, Norway*
[b]*Institute for Energy Technology, N2007 Kjeller, Norway*
[c]*Statoil, N7004 Trondheim, Norway*

Received 14 April 1996; received in revised form 30 May 1999

Abstract

An isokinetic probe has been built to obtain samples of the gas/droplet flow in oil/gas and water/gas flow. Experiments have been performed at gas densities from 22 to 47 kg/m^3, at superficial gas velocities from 3.5 to 7 m/s, but at only one superficial liquid velocity of 0.25 m/s. Samples obtained show an exponential distribution of droplets above the liquid layer in stratified flow. The liquid distribution along the vertical axis through the pipe centre is remarkably smooth in both cases, and no discontinuity in liquid flux is seen at the transition from the gas/droplet zone to the wave/bubble zone. The determination of the gas–liquid interface is the major source of uncertainty when local droplet fluxes are integrated to give a total droplet mass flow and entrained fraction. However, the wave tops can be detected from quickly increasing pressure fluctuations at the probe tip. The entrained fraction increases with the gas density to the first order and with the gas velocity to the third order. The entrained fraction is almost two times higher in the case of oil/gas than water/gas flow. Velocity profiles are obtained from stagnation pressures indicating a significant increase in gas wall friction due to droplets deposited on the wall, thereby increasing the wall roughness.

Keywords: Two-phase flow; Droplet fluxes; Isokinetic sampling; Entrained fraction; Liquid transport; High density gas

* Corresponding author. Present address: SINTEF Applied Chemistry, Department of Chemical Engineering, N-7465 Trondheim, Norway.

0301-9322/00/$ - see front matter
PII: S0301-9322(99)00054-3

1. Introduction

In order to design multiphase transport lines, the pressure drop and liquid holdup are needed for relevant phase velocities and pressures. For this purpose, the various modes of liquid transport must be described if we are going to determine how liquid accumulates in the pipeline. Liquid flowing as droplets has a velocity close to the local gas velocity, which is much higher than the velocity of the liquid layer at the bottom of the pipe, where we usually find the major part of the liquid volume fraction in a given cross section. Thus, even if the volume fraction of droplets is minute, this mode of transport is very efficient and can be of great importance.

The pressure drop available for a transport line is usually quite limited. The upper limit is given by nature through the reservoir properties. This maximum is strongly reduced by practical and economical considerations related to the design and operation of the process system receiving the fluids being transported. Thus, the designer is usually confronted with a pressure drop somewhat less than he might desire in order to achieve trouble free operation of the line under all conditions. This has the important consequence that the gas velocities are usually quite low. Superficial gas velocities below 10 m/s are common, and velocities down to 1–2 m/s may occur at reduced production. On the other hand, the gas density is high, so the interface forces may still be quite high.

Almost all studies of droplet generation use very high gas velocities and low pressures. Typically they use velocities from 15 to 100 m/s, and pressures of 1 to 3 bar. Such studies may be of immediate use to designers of high velocity systems, but should be regarded with suspicion by a designer of oil and gas transport lines until proof of their applicability is available.

The main reason for droplet studies using high gas velocities is of course of a practical and economical nature. Attaining high gas density using high pressure or a high molecular weight gas is generally more complicated and expensive than using low pressure air. High pressure not only makes the loop more expensive, but all kinds of observation and sampling of the flow become very expensive. It is, therefore, very tempting to simplify things by substituting high gas velocity for high gas density in order to achieve similar interface forces, that is the term $\rho_G U_G^2$ should be the same, where ρ_G is the gas density and U_G is the gas velocity. This could be permissible and a good alternative to more expensive methods. However, due to the importance of droplet transport, and the remoteness of these high velocity conditions to the field applications, this alternative should be examined closer. For example, the droplet velocity and momentum will be very high in these kinds of experiments. One may well ask if a velocity limit will be reached above which droplets splashing into the liquid layer will generate new droplets. If this limiting velocity is above the transport velocities, but within the range of the low pressure experiments, the results will be misleading.

Therefore, it was decided to perform an investigation using a high density gas to study the transport of droplets. In such a system some important aspects of a field transport line can be realised, as the density of the gas approaches the density of many high pressure systems. From previous work we had visual confirmation that droplets were generated at realistic (fairly low) velocities. Also the appearance of the liquid surface, both small short waves and larger waves appear very different from what is seen in low pressure air liquid systems.

It is however, realised that important aspects of real systems are not reproduced in the loop. We are mainly concerned about the gas–liquid interface tension and the liquid viscosities. Both may have very much lower values in a real system than we can obtain. Especially the interface tension is important to the droplet generation, but both fire safety and pressure limits in our system prevent further realism in these parameters.

2. The experimental facilities

2.1. The loop

The loop has previously been described by Nuland and Lingelem (1993). It has a 20 m long experimental section of 0.1 m inner diameter. It can be inclined, but in this work only the horizontal position has been used. It circulates a high molecular weight gas, sulphurhexafluorid, SF_6, which at 8 bara reaches a density of about 50 kg/m^3. This is equivalent to natural gas at about 60 bar. At 8 bara transparent PVC pipes are available. This allows visual observation of the flow, which aids the understanding of the quantitative results, although no optical technique is used in this study.

The oil enters the test section horizontally at the end of the entrance section, while the gas enters at the upper side of the entrance section, at an angle of about 45° with the pipe axis. The water enters at the lower side of the entrance section, at an angle of about 45° with the pipe axis. By this arrangement we try to create a stratified flow at the inlet of the test section. In an earlier study we have moved a transparent section close to the inlet, and judged by the visual appearance it seemed to work well.

The loop is equipped with a broad beam gamma densitometer, as described by Skarsvåg et al. (1986). This has been used both to estimate the average liquid holdup and the wave heights. At the inlet, the gas flow rate is measured by a vortex flow meter, the oil flow rate is measured with a rotameter, and the water flow rate is measured with an electromagnetic flow meter.

2.2. The fluids

The fluids used are Exxsol D80 as oil phase and sulphurhexafluorid as gas phase or alternatively water and sulphurhexafluorid. The density of the gas is given in Table 1 for relevant pressures at 20°C. The fluid properties have been found by extrapolating liquid properties at atmospheric pressure to the relevant pressures through the use of the Peng-Robinson EOS. Similarly for the gas phase, molecular weight and critical properties have been used to find properties at the relevant pressures and temperatures. The density of Exxsol D80 and water are close to 820 and 1000 kg/m^3, respectively, but a slight increase in liquid densities

Table 1
Gas densities, ρ_G, at 20°C for various absolute pressures, p_{abs}

p_{abs} (bar)	3.5	3.6	3.7	3.8	5.0	6.0	6.9
ρ_G (kg/m^3)	22.7	23.4	24.0	24.7	32.5	40.0	46.5

is seen due to gas dissolving in the liquid. The viscosity of the oil phase is 0.0016 Pa, and the surface tension is 0.022 N/m. The water has been in contact with the oil phase and this has changed the surface tension, 0.045 N/m is found as an average value, versus 0.073 N/m for pure water.

2.3. The isokinetic probe

The main parts of the isokinetic probe for flow sampling are shown in Fig. 1. It consists of a spool piece, b, that can be installed in the loop when droplet measurements are performed. A sampling tube, a, can be traversed from the bottom of test pipe to the top using a mechanism, f, which keeps track of position changes. Samples of the flow are drawn through the test tube to a small separator, i. From the separator the gas is passed on to the low pressure side of the loop. A glass window, o, is used to control the efficiency of the separator. The liquid flows from the separator into a glass measuring cylinder, j, which must be removed for emptying

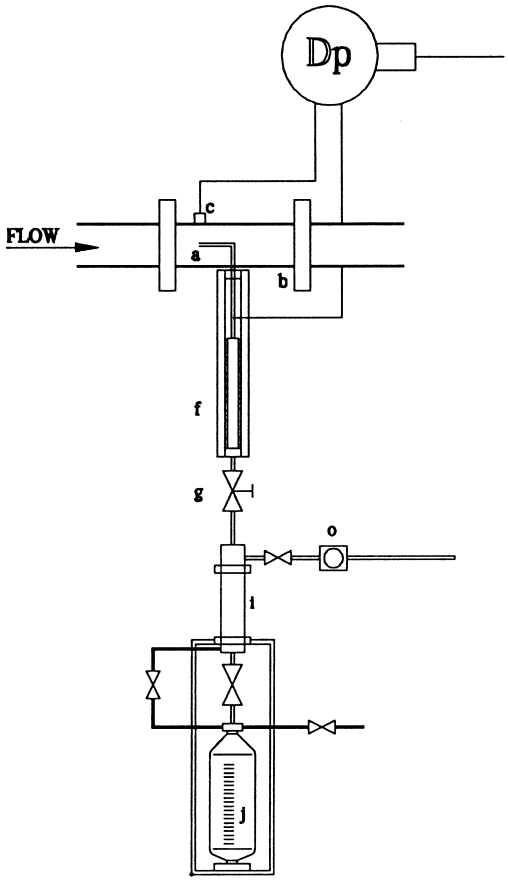

Fig. 1. Schematic of the isokinetic sampling probe.

after measurement. The manually operated valve, g, controls the rate of withdrawal through the sampling pipe and is used to assure isokinetic conditions.

The inside of the separator, i, is made as smooth as possible to prevent liquid from accumulating there. Starting an experiment, a period of stable flow is allowed before starting to measure the rate of accumulation of liquid, to eliminate the effect of initial accumulation of liquid on surfaces.

Fig. 2 shows the sampling tube in some detail. The tube has two channels, one central that is used to draw samples and one annular for pressure measurement. The central channel has an inner diameter of 3.2 mm, which was chosen to be larger than the estimated maximum size of droplets which was 2 mm (visual observation of droplets hitting the pipe wall and some pictures taken indicate that most droplets are smaller than 1 mm except perhaps very close to the liquid surface).

The annular channel opens to the central channel at the tip of the tube and can be connected to a differential pressure-cell, Dp, below the pack box and sealing mechanism. The other side of the differential pressure-cell is connected to an opening at the top of the spool piece, c in Fig. 1. There is a connection to high pressure gas which is used to clean the pressure tappings when a new sampling is prepared.

The channels used to measure the pressure difference are usually filled with some liquid after sampling for some time. It is, therefore, a limited time available to adjust the flow to isokinetic conditions. We let the valve stay in the proper position, ignore pressure variations which are now due to liquid entering the pressure tappings, and measure the rate of accumulation of liquid in the glass cylinder. The sensitivity of the measured volume flux of droplets to the

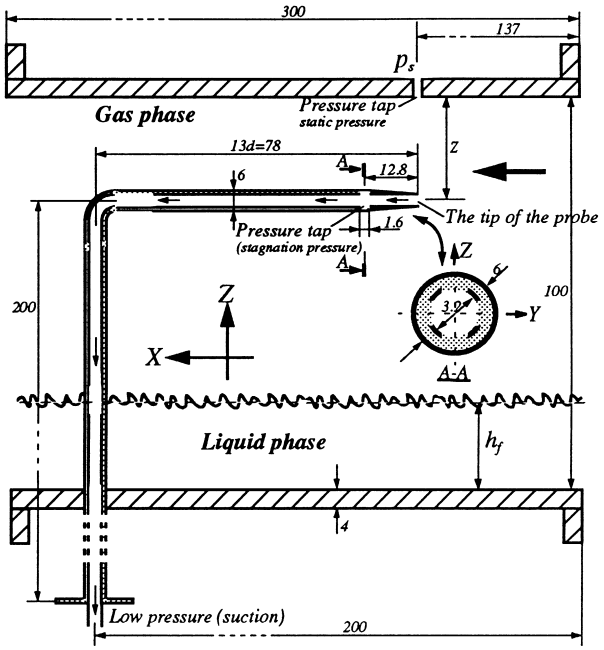

Fig. 2. Details of the isokinetic sampling probe.

departure from isokinetic condition is tested by imposing a known pressure difference Δp, in the same order as variations in the stagnation pressure. The tests show that for small departures from isokinetic condition the change in measured liquid rate can be ignored. In the cases tested here, a deviation from isokinetic conditions of $\pm 50\%$ of the stagnation pressure gives about $\pm 13\%$ change in the measured liquid flux. Consequently the results are not very sensitive to achieving an exact isokinetic condition, a fact also observed by Williams (1990). Thus it is not important to monitor the isokinetic condition during the whole sampling period.

The isokinetic probe is placed 100 diameters downstream from the inlet. This should be sufficient to achieve constant deposition and entrainment rates according to Leman (1985). In the remaining transparent part of test section there is no visible change in liquid level, except for the last meter before the outlet. This supports the assumption that there is no substantial change in the droplet transport over this distance.

To check the results, the probe was also used as a pitot tube to obtain the velocity distribution in the liquid layer. The total liquid transport is estimated, and summed up to the input rate. Because of the changes between phases in the wave region the stagnation pressure varies due to the varying hydrostatic pressure and dynamic pressure. This makes it difficult to measure the liquid velocity in the wave region by using the probe. So we integrate the velocity profile in the liquid layer from the bottom of the pipe to the lower edge of the wave region, $h_{\min}$, Fig. 3. This means that the liquid transport by the waves is not measured, because it is impossible to get a reliable measurement of the stagnation pressure. Even if a kind of estimate of the liquid velocity could be obtained, an estimate of the local phase fractions would not be possible. Total liquid transport was estimated by summing up the measured liquid transport by droplets above the wave tops and the transport in the liquid layer below the waves. This sum is almost 3.5% less than the total liquid input rate. The uncertainty is mainly due to the liquid transport by the waves which is not accounted for.

The probe measures the local volume flux of droplets. To obtain an estimate of the local droplet volume fraction, we measure the stagnation pressure for every position where we measure the droplet flux. From these data we can find the gas velocity and the droplet volume fraction. However, for model development we are mainly interested in the droplet volume flux.

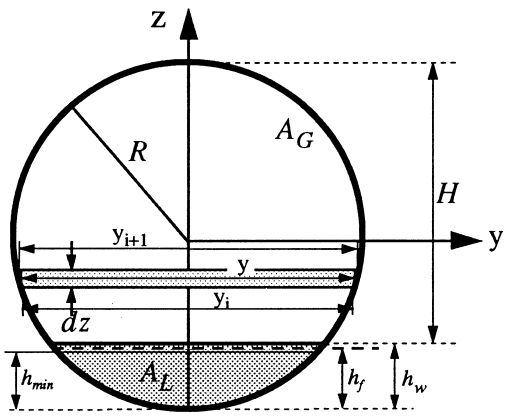

Fig. 3. Sketch of the limits for the integration of the droplet flux.

3. Results

3.1. The flow regime

The flow regimes in all of these experiments are a kind of stratified wavy flow. There is no sign of transition to annular flow through upcreeping or liquid spilling up on the side of the pipe wall. Rather the surface of the liquid is on the average flat in the direction transverse to the flow direction. However, there is a thin, wavy liquid film covering the pipe wall above the liquid level. This film seems to move very slowly, of the order of mm/s, its contribution to liquid transport is, therefore, negligible.

3.2. Spatial distribution of droplets and determination of the liquid interface

Fig. 4 shows the results of two typical series of sampling. A dotted horizontal line indicates the position of the first measurement above the wave tops. In this and other figures showing spatial distribution 0 of the scale is in the centre of the pipe. The continuity of the liquid flux across this boundary was a surprise to us. From the flux measurements alone we are not able to tell if the sampled liquid represents droplets or waves. In order to know if the liquid we sample is from droplets, waves or a foamy layer on top of the continuous liquid phase, the position of the wave tops must be determined by other means. We have used the stagnation pressure measured with the probe which starts to fluctuate when the wave tops hits the probe tip.

The liquid volume fraction from the broad beam gamma densitometer can be converted to a liquid height using geometry and assuming that the liquid surface is flat (normal to the pipe axis) and that the liquid forms a compact layer with no gas bubbles. From the appearance of the flow, the first assumption seems to be a fair one. Small amounts of liquids wet the upper part of the pipe, but its effect on the calculated liquid height must be minute. The second assumption, however, is more dubious as a lot of gas bubbles apparently are entrained in the

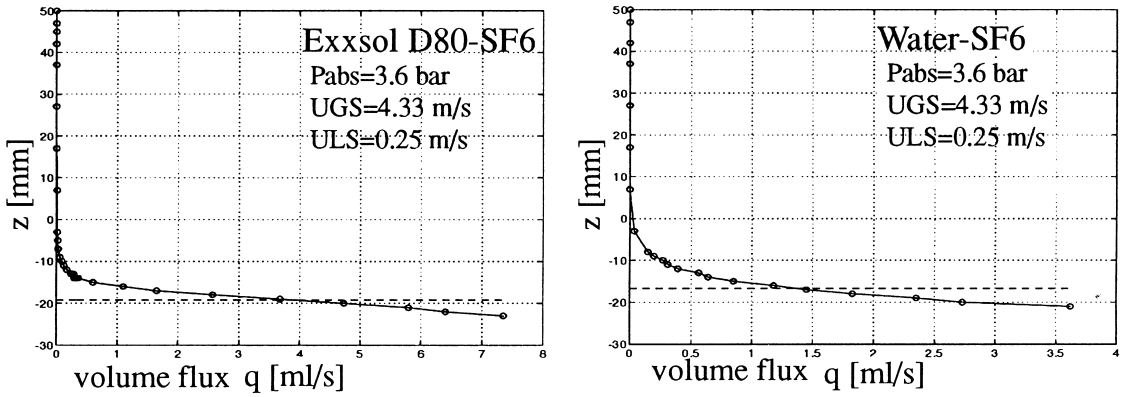

Fig. 4. Local volume flux profile of droplets at $U_{GS} = 4.33$ m/s, $U_{LS} = 0.25$ m/s, $p_{abs} = 3.6$ bar, $\rho_G = 23.4$ kg/m^3. The dashed line indicates the first sampling position above the wave tops.

liquid causing the liquid surface to rise. As we have no means to determine the amount of gas bubbles, the liquid level evaluated from the gamma densitometer measurement must be too low.

When the stagnation pressure is measured in what is clearly gas/droplet flow, we observe a constant pressure. As we approach the liquid level we see that at a certain position, the stagnation pressure starts to oscillate. Judging from the visually observed liquid level and the position of the probe (note that we can not see the probe tip), this must be wave crests hitting the probe. Therefore, we have used this position as the lower limit for the gas droplet flow. Fig. 5 shows the maximum liquid level as a function of pressure and superficial gas velocity for oil/gas and water/gas. The two methods for evaluating the surface position agree at low velocities. At higher velocities we can observe bubbles being mixed into the liquid layer. The appearance of the liquid also changes at higher velocities, from being clear and transparent to grey and opaque. In parallel with these visual signs of bubble entrainment, we observe an increasing difference between the level observed with the probe and the one indicated by the gamma densitometer. Using higher flow rates this becomes even more dominating, in extreme cases we observe a holdup of around 40% though the gamma densitometer, while we visually observe an apparent liquid level corresponding to a holdup of about 80% (Lunde and Nuland, 1997). Evidently more bubbles are entrained with increasing gas velocity and increasing pressure as these visual observations confirm. This must have an effect on the gas flow above the liquid (foam) layer. The pipe cross section available for gas transport is restricted, and, therefore, the velocity and the friction is increased.

The liquid surface is quite different for oil/gas and water/gas under otherwise equal

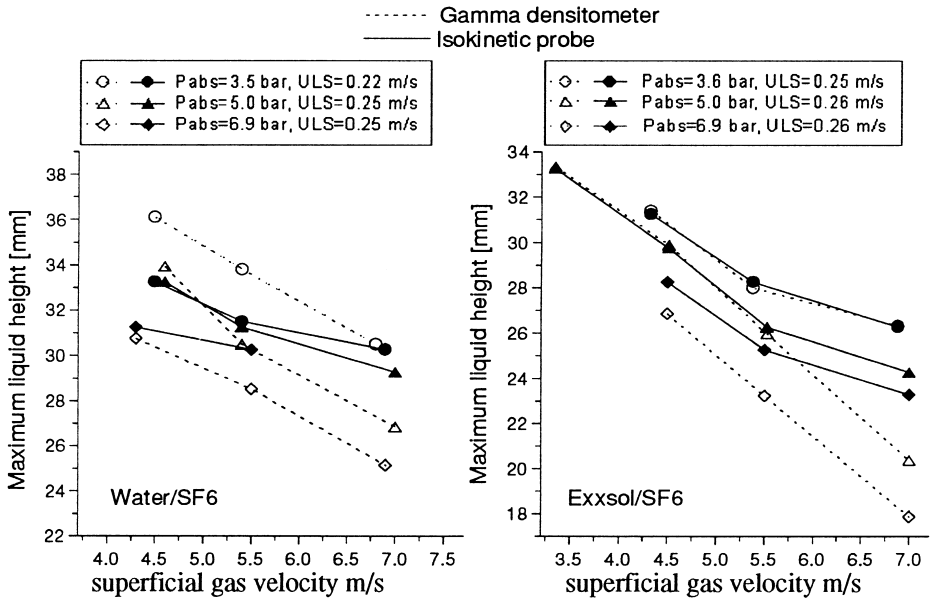

Fig. 5. Comparison between measurements of maximum liquid film height made by the isokinetic sampling probe and the broad beam gamma densitometer.

conditions. Fig. 6 shows examples of time series measurements made by the broad beam gamma densitometer for oil/gas and water/gas. The wave amplitude in the water case is more than two times larger than those in the oil case. Tables 2 and 3 show the wave height, standard deviation and sampling frequency for both oil/gas and water/gas, respectively. The differences may be due to the difference in surface tension. The wave height may be limited by the droplet generation. A higher surface tension reduces the droplet generation and allows a greater wave height and higher local gas velocity before liquid removal balances the wave generating forces.

3.3. Integration of droplet flux

In order to obtain the total droplet mass flux, we integrate the droplet flux distribution above the limiting position determined through the stagnation pressure. First the local flux distribution is fitted using a sum of two exponential distributions. Then we assume that the flux is constant across the pipe along a line normal to the vertical axis traversed with the probe. This assumption is supported by observations by Paras and Karabelas (1991). The local fluxes are then integrated across the gas cross section, Fig. 3. The results of the integrations, together with the experimental conditions, are given in Table 4 for oil/gas and Table 5 for water/gas. The entrained fraction, E, is also given. This is defined as the fraction of the liquid

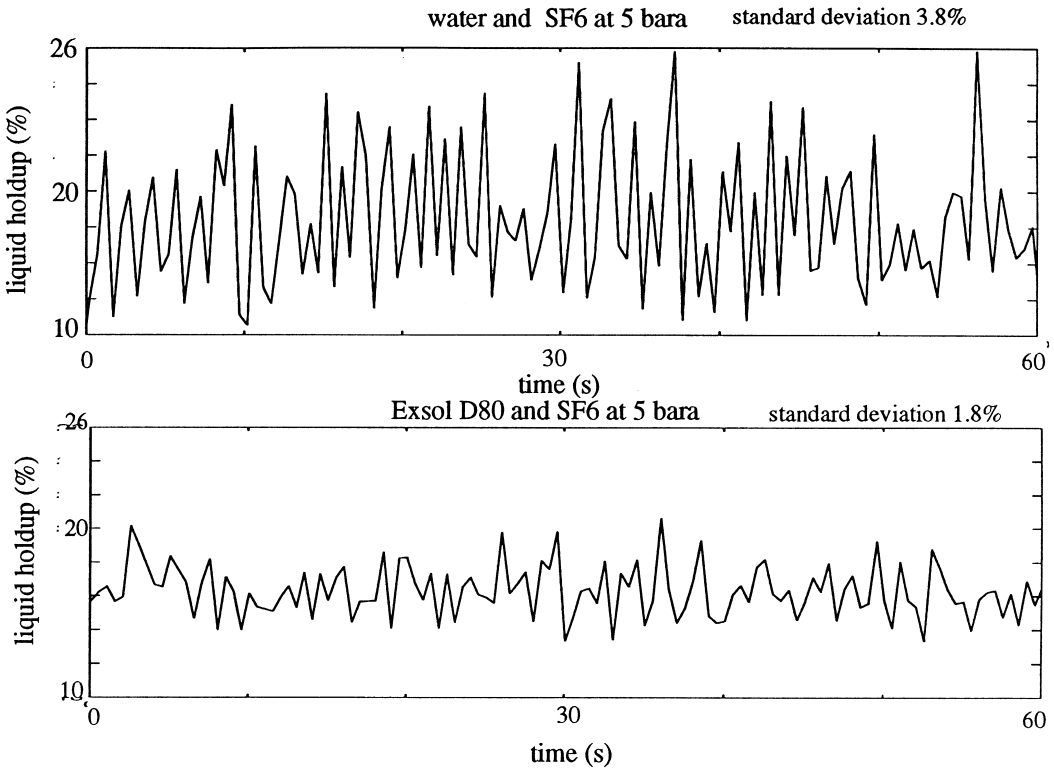

Fig. 6. Time series of liquid holdup from the broad beam gamma densitometer.

Table 2
Wave height Δh_{wo}, standard deviation σ'_o, and sampling frequency f, from the broad beam gamma densitometer for various gas/liquid flow rates at different pressures

Exxsol D80/SF6					
U_{GS} (m/s)	U_{LS} (m/s)	ρ_G (kg/m^3)	Δh_{wo} (mm)	σ'_o (mm)	f (Hz)
4.33	0.25	23.4	5.17	3.916	5
5.38	0.25	23.4	6.95	4.503	5
6.89	0.25	23.4	8.45	4.503	5
7.03	0.26	24.05	7.09	4.503	5
3.35	0.26	32.5	5.19	3.916	2
4.51	0.26	32.5	8.28	4.503	2
5.53	0.26	32.5	6.88	4.311	2
7.00	0.26	32.5	4.17	2.827	2
4.5	0.26	40.0	7.10	4.59	2
4.5	0.26	46.5	6.09	4.69	2
5.5	0.26	46.5	4.44	5.055	2
7.0	0.26	46.5	3.42	2.331	2

being transported as droplets:

$$E = \frac{W_{LE}}{W_L} \tag{1}$$

3.4. Droplet distribution

To study the effect of the gas velocity on the volume flux of droplets, the experiments were

Table 3
Wave height Δh_{wo}, standard deviation σ'_o, and sampling frequency f, from the broad beam gamma densitometer for various gas/liquid flow rates at different pressures

Water/SF6					
U_{GS} (m/s)	U_{LS} (m/s)	ρ_G (kg/m^3)	Δh_{wo} (mm)	σ'_o (mm)	f (Hz)
4.5	0.22	22.75	16.50	6.725	5
5.4	0.22	22.75	16.41	6.881	5
6.8	0.24	24.70	16.84	7.931	5
7.0	0.22	22.75	14.31	7.339	5
4.6	0.25	32.50	14.76	7.489	2
5.4	0.25	32.50	14.20	8.075	2
7.0	0.25	32.50	14.84	7.188	2
4.3	0.25	46.5	11.77	7.035	2
5.5	0.25	46.5	14.75	7.188	2
6.9	0.25	46.5	11.49	7.785	2

Table 4
Summary of experimental conditions and results for oil/gas. U_{GS} is superficial gas velocity, U_{LS} is superficial liquid velocity, U_G is gas velocity, U_L is liquid velocity, ρ_G is gas density, p_{abs} is absolute pressure, h is liquid holdup, h_f, h_{max} and h_{min} are mean, maximum and minimum liquid height measured by the broad beam gamma densitometer respectively. $|dp/dx|$ is the magnitude of pressure gradient, W_L, W_{LE} W_{LF} are mass flow rate of the liquid, the entrained liquid and the liquid film respectively. E is the entrained liquid fraction

Exxsol D80/SF6

U_{GS} (m/s)	U_{LS} (m/s)	U_G (m/s)	U_L (m/s)	ρ_G (kg/m^3)	p_{abs} (bar)	h %	h_f (mm)	h_{max} (mm)	h_w (mm)	$\lvert\frac{dp}{dx}\rvert$ (Pa/m)	W_{LE} (kg/s)	W_L (kg/s)	W_{LF} (kg/s)	E (%)
4.33	0.25	5.68	1.03	23.4	3.6	23.7	28.68	31.39	31.25	88	0.044	1.59	1.55	2.79
5.38	0.25	6.66	1.24	23.4	3.6	19.2	24.68	27.98	28.25	125	0.081	1.59	1.51	5.07
6.89	0.25	8.17	1.45	23.4	3.6	15.7	21.42	26.30	26.25	192	0.142	1.59	1.45	8.91
7.03	0.26	8.35	1.48	24.05	3.7	15.8	21.51	25.05	25.75	206	0.163	1.65	1.49	9.85
3.35	0.26	4.52	0.99	32.5	5.0	25.9	30.57	33.35	33.25	98	0.027	1.65	1.63	1.65
4.51	0.26	5.64	1.25	32.5	5.0	20.0	25.41	29.89	29.75	117	0.070	1.65	1.58	4.25
5.53	0.26	6.61	1.45	32.5	5.0	16.3	21.99	25.95	26.75	160	0.151	1.65	1.50	9.11
7.00	0.26	8.01	1.80	32.5	5.0	12.6	18.37	20.35	24.25	240	0.215	1.65	1.44	13.03
4.5	0.26	5.56	1.30	40.0	6.0	19.1	24.64	28.37	28.75	147	0.097	1.65	1.56	5.86
4.5	0.26	5.51	1.33	46.5	6.9	18.3	23.86	26.84	28.25	188	0.111	1.65	1.54	6.73
5.5	0.26	6.48	1.51	46.5	6.9	15.1	20.84	23.21	25.25	286	0.205	1.65	1.45	12.37
7.0	0.26	7.86	1.84	46.5	6.9	10.9	16.81	17.86	23.25	431	0.380	1.65	1.27	22.97

Table 5
Summary of experimental conditions and results for water/gas. U_{GS} is superficial gas velocity, U_{LS} is superficial liquid velocity, U_G is gas velocity, U_L is liquid velocity, ρ_G is gas density, p_{abs} is absolute pressure, h is liquid holdup, h_f, h_{max} and h_{min} are mean, maximum and minimum liquid height measured by the broad beam gamma densitometer respectively. $|dp/dx|$ is the magnitude of pressure gradient, W_L, W_{LE} W_{LF} are mass flow rate of the liquid, the entrained liquid and the liquid film respectively. E is the entrained liquid fraction

Water/SF6

U_{GS} (m/s)	U_{LS} (m/s)	U_G (m/s)	U_L (m/s)	ρ_G (kg/m^3)	p_{abs} (bar)	h %	h_f (mm)	h_{max} (mm)	h_w (mm)	$\lvert\frac{dp}{dx}\rvert$ (Pa/m)	W_{LE} (kg/s)	W_L (kg/s)	W_{LF} (kg/s)	E (%)
4.5	0.22	5.68	1.05	22.75	3.5	20.78	26.11	36.07	33.25	94.9	0.017	1.728	1.71	1.0
5.4	0.22	6.53	1.26	22.75	3.5	17.26	22.89	33.02	31.5	131	0.026	1.728	1.70	1.52
7.0	0.22	8.16	1.46	22.75	3.5	14.21	19.97	28.07	30.25	186	0.10	1.728	1.63	5.78
6.8	0.24	7.97	1.55	24.70	3.8	14.66	20.41	30.49	30.25	186	0.105	1.885	1.78	5.59
4.6	0.25	5.72	1.25	32.50	5.0	19.63	25.07	33.93	33.25	138.4	0.042	1.964	1.92	2.12
5.4	0.25	6.45	1.46	32.50	5.0	16.33	22.02	30.49	31.25	179.7	0.094	1.964	1.87	4.78
7.0	0.25	8.03	1.78	32.50	5.0	12.82	18.58	26.84	29.25	245	0.169	1.964	1.80	8.63
4.3	0.25	5.30	1.27	46.5	6.9	18.90	24.41	30.74	31.25	142	0.075	1.964	1.89	3.8
5.5	0.25	6.48	1.56	46.5	6.9	15.16	20.90	28.51	30.25	209	0.112	1.964	1.85	5.71
6.9	0.25	7.86	—	46.5	6.9	12.16	17.92	25.14	–	304	–	–	–	–

made with superficial gas velocities in the range of 3.3–7 m/s, at constant gas density. Fig. 7(A) shows an example of the local volume flux of droplets q, as a function of superficial gas velocity U_{GS}, and constant gas density ρ_G. A short horizontal line indicates the position where the first sampling is made above the wave crests in each case. By judging the integral under the

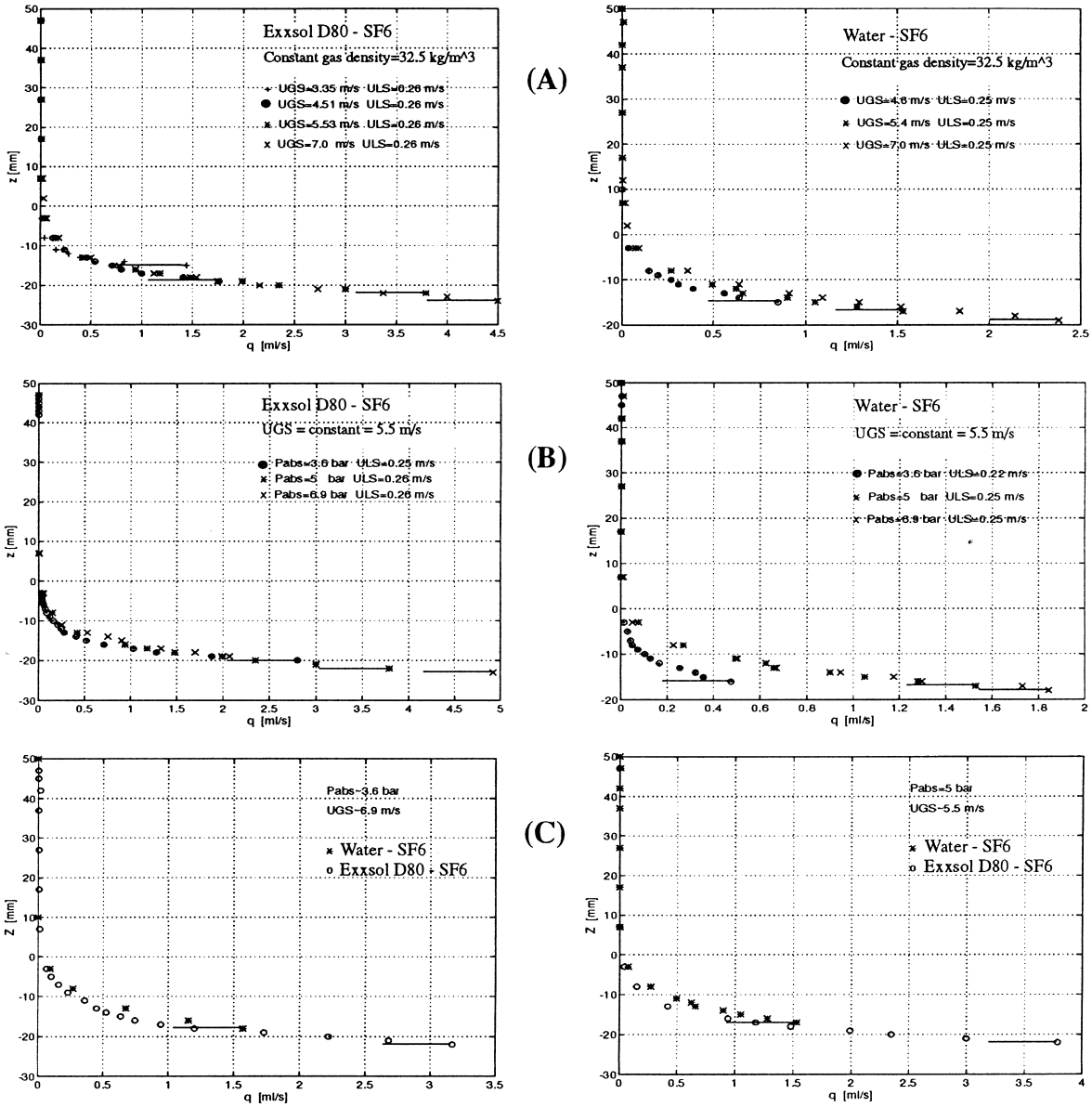

Fig. 7. Local volume flux of droplets for (A) different gas velocities at constant gas density, (B) different gas densities at constant gas velocity, (C) different liquids at constant gas velocity and gas density. For each series of measurements a short horizontal line indicates the position of first sample above the wave crests.

curves one can see that an increase in gas velocity causes an increase in the liquid transport by droplets.

By keeping the gas rate constant and varying the gas density in the range of 22–47 kg/m^3, we study the effect of gas density on the liquid droplet transport. Fig. 7(B) shows an example of the local volume flux of droplets q, as a function of gas density ρ_G, at constant gas rate U_{GS}. It is evident how an increase in gas density leads to an increase in droplet liquid transport. Note that the vertical position, z, is measured from the center of the pipe.

The increase in droplet transport with gas velocity (Fig. 7(A)) or gas density (Fig. 7(B)), is due to the fact that more of the pipe cross section becomes available to the droplets. At a certain position in the pipe, relative to the pipe walls, the local droplet volume flux is almost independent of gas velocity or pressure. The local droplet flux at a given distance above the wave crests, however, increase with increasing gas velocity and gas density.

A comparison is made between droplet transport in oil/gas and water/gas by using to different type of liquids (Exxsol D80 and water) as liquid phase under the same conditions. These combinations are made to study the effects of liquid phase on droplet transport. Fig. 7(C) shows two examples of the local droplet liquid flux of oil/gas and water/gas at constant gas rates and gas densities. The difference in droplet liquid transport caused by liquid type is easy to see in Fig. 7(C).

The distributions of droplet fluxes have exponential forms. A function with two exponential components is used to fit the data.

$$q(z) = \beta_1 \cdot \exp(-\lambda_1 \cdot z) + \beta_2 \cdot \exp(-\lambda_2 \cdot z) \tag{2}$$

where β_1 and β_2 are amplitude coefficients, and λ_1 and λ_2 are 'decay' coefficients.

The two decay coefficients are needed due to the extreme differences in droplet fluxes in the area near the liquid surface and the upper part of the pipe. It seems that we may have two families of droplets, i.e. a distribution with two maxima. The smaller droplets spread more evenly across the pipe cross section.

The four constant fits are used for the (numerical) integration to obtain the total droplet fluxes. However, this mathematical form is hard to interpret physically. By accepting a poorer fit to the minute fluxes in the upper part of the pipe we can use a two constant fit as in Eq. (3). The experiments show that the effect of the droplet flux in the upper part of the pipe cross section is very small.

$$q(z) = \beta^* \cdot \exp(-\lambda^* \cdot z) \tag{3}$$

where β^* is an amplitude coefficient and λ^* is a decay coefficient.

The coefficients β^* and λ^* are determined using the least square method, and are shown in Tables 6 and 7 for oil/gas and water/gas, respectively. Increasing the gas rate or the gas density, the value of the coefficient β^* increases and the value of the coefficient λ^* decreases. Increasing β^* and decreasing λ^* means a larger area under the curve for q, which again means more liquid transport in the form of droplets.

Table 6
Coefficients for curve fitting to the oil/gas measurements. β^* is an amplitude coefficient, λ^* is a decay coefficient, λ is the 'decay' coefficient determined based on the measurements of the local droplet concentrations and ζ is the dimensionless droplet diffusivity

Exxsol D80/SF6						
U_{GS} (m/s)	U_{LS} (m/s)	ρ_G (kg/m^3)	β^*	λ^*	λ	ζ
4.33	0.25	23.4	1.328	0.409	0.409	0.44
5.38	0.25	23.4	2.166	0.261	0.263	0.44
6.89	0.25	23.4	2.915	0.200	0.199	0.34
7.03	0.26	24.05	3.110	0.186	0.189	0.34
3.35	0.26	32.5	0.990	0.388	0.389	0.72
4.51	0.26	32.5	1.745	0.239	0.240	0.73
5.53	0.26	32.5	3.841	0.236	0.238	0.50
7.00	0.26	32.5	4.923	0.206	0.206	0.35
4.5	0.26	40.0	2.449	0.258	0.258	0.67
4.5	0.26	46.5	2.293	0.252	0.252	0.65
5.5	0.26	46.5	5.112	0.229	0.230	0.46

3.5. Comparison with the droplet distribution model of Paras and Karabelas

The measurements of droplet distribution in this study can be compared with a model proposed by Paras and Karabelas (1991) as follows:

$$C = \beta \cdot \exp\left(-k\frac{z}{R}\right) = A + \beta \cdot \exp(-\lambda \cdot z), \quad \lambda = \frac{k}{R} \tag{4}$$

where $C(z) = Q_d(z)/U_G(z)$ is the local concentration of droplets, Q_d is the local mass flux of

Table 7
Coefficients for curve fitting to the water/gas measurements. β^* is an amplitude coefficient, λ^* is a decay coefficient, λ is the 'decay' coefficient determined based on the measurements of the local droplet concentrations and ζ is the dimensionless droplet diffusivity

Water/SF6						
U_{GS} (m/s)	U_{LS} (m/s)	ρ_G (kg/m^3)	β^*	λ^*	λ	ζ
4.5	0.22	22.75	0.271	0.394	0.392	0.92
5.4	0.22	22.75	0.650	0.273	0.274	0.87
6.8	0.24	24.70	1.667	0.189	0.188	0.80
7.0	0.22	22.75	1.821	0.223	0.222	0.63
4.6	0.25	32.50	0.891	0.261	0.262	1.27
5.4	0.25	32.50	1.641	0.212	0.212	1.13
7.0	0.25	32.50	2.810	0.203	0.203	0.71
4.3	0.25	46.5	1.463	0.231	0.231	1.833
5.5	0.25	46.5	2.061	0.220	0.220	1.12

droplets, β is an 'amplitude' constant, R is the pipe radius, z is the vertical position. A is apparently very small or zero as the droplet fraction is very small a sufficient distance from the surface. k is defined as follows:

$$k \equiv \frac{wR}{\varepsilon} = \frac{w}{\zeta U^*} \tag{5}$$

where w is the droplet settling velocity and ε is the eddy diffusivity given by $\varepsilon = \zeta \cdot R \cdot U^*$ where ζ is the dimensionless droplet diffusivity and U^* is the friction velocity. λ is the 'decay' coefficient determined based on measurements of local concentration of droplets and its values given in Tables 6 and 7.

We calculate the droplet settling velocity, w, using the same method as Paras and Karabelas (1991) due to Wallis (1975). The friction velocity is used to find the eddy diffusivity, however, the authors do not describe under which assumption this is found. We have assumed that the shear stress is the same around the gas perimeter, and calculate this shear stress on the basis of the measured pressure drop. The gas cross sectional area and the wall and interface perimeters are calculated on the basis of gamma densitometer phase fractions, and assuming the flow is stratified with a flat surface normal to the pipe axis. This is in accord with what we can observe visually. With these assumptions, the friction velocity is:

$$U^* = \left(\frac{A_G}{S_i + S_G} \left(\frac{\partial p}{\partial x} / \rho_G \right) \right)^{0.5} \tag{6}$$

where A_G is the gas cross sectional area, S_i is the interface perimeter and S_G is the gas perimeter against the pipe wall. The apparent droplet diffusivities of Tables 6 and 7, vary considerably with pressure, velocity and type of liquid. In all these experiments the gas flow appears more effective in lifting the droplets than the literature value for diffusivity, $\zeta = 0.1$ indicates. (It should be noted that we as a convenience refer all discrepancies to diffusivity coefficient, although it could as well result from errors in the droplet size and the ensuing settling velocity.) This may be due to limitations in the model, especially the assumption of homogenous turbulence, which may be a better assumption in the Paras and Karabelas experiments. In their experiments the liquid film thickness is roughly the same around the pipe perimeter, and the wave height is negligible compared to the pipe diameter. In the present experiments, the film and, therefore, the surface roughness is highly asymmetrically distributed. At the surface of the liquid layer, where the droplets are generated, the wave heights are of the order of centimetres, while on the thin film covering the upper part of the pipe periphery, the waves are of submillimeter heights. Although, at present the shear stress distribution has not be measured, it appears that it must be much higher where the droplets are generated. Probably an even more uneven distribution of shear stress than found by Paras et al. (1994). The average pressure drop may not be representative for the turbulent activity just at the spots where the droplets are mainly formed and the hypothesis of an average shear stress around the gas perimeter, underestimate the turbulence intensity just where the droplets are generated.

Thus it is proposed that the discrepancy between the diffusivity found in these experiments and in literature is due to concentration of turbulent activity: first a concentration along the

gas perimeter to where the roughness is highest, then a concentration at the wave crests where the gas cross section is significantly reduced.

Larger, millimetre sized droplets are also visible on high speed films of the experiments, these are clearly not governed by diffusion, and may, therefore, change the droplet distribution away from that predicted by theory. Vames and Hanratty (1988) found that for larger droplets (150 μm) the lift force, Saffman (1965) plays a role:

$$F_l = \frac{K\mu_G}{\nu_G} d_d^2 \left|\frac{dU}{dr}\right|^{1/2} (U_G - U_d) \tag{7}$$

where K is the constant of proportionality, μ_G is the dynamic gas velocity, ν_G is the kinetic gas viscosity, d_d is the droplet diameter, U_G is the gas velocity and U_d is the droplet velocity. In our case the droplet diameter and the velocity difference are probably much greater than in the experiments of Vames and Hanratty (1988), and the contribution from this force to the droplet distribution may be significant.

It should also be noted that Paras and Karabelas can assume symmetric velocity distribution with relatively small velocities at the wall, due to the thin film. In our case the velocity profile is quite asymmetric, with a significant velocity at the interface. This may give the droplets a certain initial velocity, possibly randomly distributed, and which contributes to an exponential distribution, adding to the apparent diffusivity.

3.6. Correlation of entrained fraction

Defining a Weber number as

$$We = \left(\rho_G U_G^2 h_w\right)/\sigma \tag{8}$$

where h_w is maximum local liquid height measured by the isokinetic sampling probe and σ is the surface tension. We introduce a correlating variable

$$xx = We\ U_G \tag{9}$$

Fig. 8 shows a plot of the entrained fraction E, against this variable.

Following Williams et al. (1966) in equating rate of entrainment and rate of deposition, and correlating the rate of deposition as

$$R_D = k_D C_D \tag{10}$$

and

$$C_D = \frac{EW_L}{Q_G S} \tag{11}$$

where R_D is the rate of deposition, W_L is mass flow rate of the liquid and S is slip between droplets and gas. It follows that the rate of entrainment, R_A, is proportional to the Weber number.

$$R_A = \frac{KWe}{S} W_L \tag{12}$$

where the constant of proportionality K, may contain all functional dependencies not examined here, notably, of liquid rate and pipe diameter.

Three important conclusions seem to be evident from these data. First, the entrained fraction is proportional to the gas density. Other correlations based on a more narrow range of gas densities, Dallman et al. (1984), use the square root of the gas density. The difference is extremely important for extrapolation to higher pressures. Second, the entrained fraction increases with the third power of the gas velocity, this is in accord with Dallman et al. (1984). For this parameter the spread in the data is higher, and a higher exponent might be defended. However, for the purpose of conservatism in design of multiphase transport lines, it is important not to overestimate the extent of droplet transport as this mode of transport is so much more effective than other forms of liquid transport. Third, the entrained fraction decreases in proportion with increasing surface tension as could be expected, this is seen from the difference between water and oil data. For the highest entrained fraction in Fig. 8, all the local measurements could not be completed due to equipment breakdown. The liquid level is, therefore, more uncertain for this data point.

It should be noted that these data have been obtained with essentially one liquid superficial velocity giving fairly small holdups. Therefore, the dependency on liquid level, and liquid flow is more uncertain, extrapolation of the correlation toward a very high holdup is not intended.

3.7. Droplet influence on gas velocity profile and wall friction

The local gas velocity is important in order to derive the local droplet concentration. It also gives a deeper insight in the physics of the flow. Fig. 9 gives an example of the local gas velocity profile as it is obtained using the probe as a pitot tube. The small circles or stars show the stagnation pressure interpreted as velocity using only the gas density. Toward the liquid

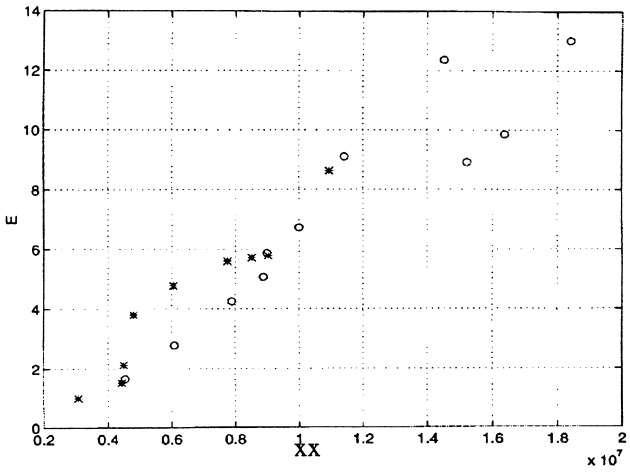

Fig. 8. Correlation of entrained fractions, E against the xx of Eq. (9). (○): oil, (∗): water.

surface we can see that the presence of droplets distort the values from a reasonable curve. However, the real mixture density should be used in interpreting the stagnation pressure

$$p_{\mathrm{d}} = \frac{1}{2}\rho_{\mathrm{m}} U_{\mathrm{G}}^2 \tag{13}$$

where p_{d} is the dynamic pressure and ρ_{m} is the mixture density. The mixture density being defined by

$$\rho_{\mathrm{m}} = h(z)\rho_{\mathrm{L}} + \big(1 - h(z)\big)\rho_{\mathrm{G}} \tag{14}$$

Here $h(z)$ means the local holdup at the position where we are calculating the velocity, so the average density used changes according to the position. We have also measured the local mass flux of droplets

$$Q_{\mathrm{d}} = h\rho_{\mathrm{L}} U_{\mathrm{G}} \tag{15}$$

This yields an equation for the local gas velocity

$$U_{\mathrm{G}} = \frac{\left(-0.5Q_{\mathrm{d}}\big(1 - \rho_{\mathrm{G}}/\rho_{\mathrm{L}}\big) \pm \sqrt{\big[0.5Q_{\mathrm{d}}\big(1 - \rho_{\mathrm{G}}/\rho_{\mathrm{L}}\big)\big]^2 + 2\rho_{\mathrm{G}} p_{\mathrm{d}}} \right)}{\rho_{\mathrm{G}}} \tag{16}$$

where only the positive root has physical significance.

The continuous line in Fig. 9 shows gas velocities based on this equation, which is much more reasonable.

The velocity profile near the wall can be related to the wall friction factor. Following Hinze (1975) we have

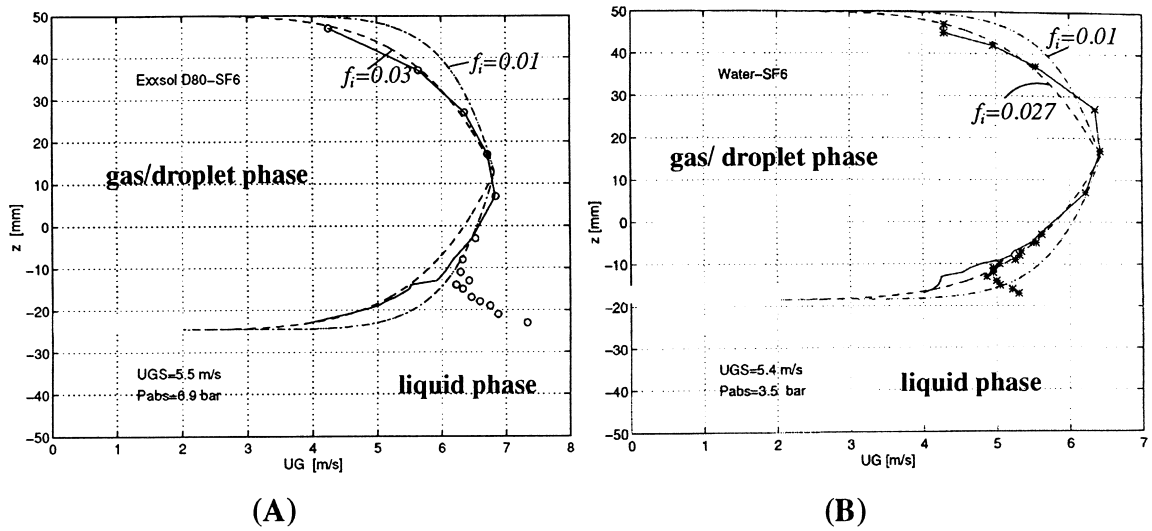

Fig. 9. Local gas velocity profiles based on stagnation pressure, (A) oil/gas and (B) water/gas.

$$\frac{U(z)}{U_{\max}(z)} = \left(\frac{2z}{H}\right)^{1/n} \tag{17}$$

and $1/n = \sqrt{f_i}$ where f_i is the Moody friction factor (Moody, 1944), and H in this work is the distance from the top of the pipe to the liquid surface. The position z is the distance from the top of the pipe. The broken lines in Fig. 9 show a comparison between the U_G of Eq. (16) and a velocity profile obtained by using Eq. (17). The maximum velocity, $U_{\max}(z)$ is obtained from the stagnation pressure measurements. The friction factor of 0.01 corresponds to the Reynolds number of the flow and a smooth pipe wall. We see that a friction factor of 0.03 for oil/gas and 0.027 for water/gas gives a better fit, indicating an appreciable increase in the wall roughness. Previous tests using dry gas have indicated that the wall is quite smooth. Visual inspection shows that the upper part of the wall is covered by a thin wavy film, estimated to be around 1 mm thick. This must be the source of the increased roughness. Comparison with a large number of stratified droplet flow cases indicate that inclusion of such a droplet generated wall roughness improve pressure predictions (Nuland, 1994).

4. Conclusion

An isokinetic probe has been built to obtain samples of gas/droplet flows. Sensitivity tests indicate that the local droplet mass fluxes obtained are representative of the true values. The major uncertainty arises when we integrate the local droplet fluxes to obtain the total droplet flux. This uncertainty is due to the waves which makes it difficult to determine the position of the liquid surface.

In order to determine the position of the wave tops as the lower integration limit, both the gamma densitometer and the stagnation pressure measured with the probe are used. The oscillating stagnation pressure is a reliable sign that the wave crests are hitting the probe. The liquid levels indicated by the probe are used when the gamma densitometer indicates a lower value for the liquid height at the bottom of the pipe.

The local droplet flux profile along a vertical pipe diameter shows an exponential distribution. These profiles are integrated by fitting a sum of two exponential functions to the local droplet flux distributions and assuming a constant droplet flux distribution along the horizontal chords of the pipe cross section. Integrating the profiles provides reliable data on the mean liquid entrained fraction E.

The Paras and Karabelas (1991) droplet diffusion model requires considerable adjustment to fit the low velocity high gas density case, and generally an increase in the dimensionless droplet diffusivity, ζ is necessary to fit the data. This means that the dense gas is more efficient in lifting the droplets than indicated by the theory.

We propose that the wavy liquid surface may introduce an extra turbulence to the gas flow, concentrated near the wave tops and near the surface, making the average diffusivity calculations of the Paras and Karabelas model less appropriate. Due to the lower gas velocity compared to the Paras and Karabelas experiments, the droplets are greater. This means that the lift force due to shear may also be important.

The results from this study show that the entrained fraction E, is proportional to U_G^3 and

ρ_G. The present data support the assumption that entrainment is inversely proportional to the surface tension, σ.

An analysis of the velocity profile indicates that the wall friction is considerably increased due to deposition of droplets causing an increased wall roughness.

Acknowledgements

The financial support of Statoil, Institute for Energy Technology and Centre of Technology at Kjeller is acknowledged. The authors also wish to thank Prof. Arnold F. Bertelsen and Knud Lunde for their assistance.

References

Dallman, J.C., Laurinat, J.E., Hanratty, T.J., 1984. Entrainment for horizontal annular gas–liquid flow. Int. J. Multiphase Flow 10, 677–690.

Hinze, J.O., 1975. Turbulence. McGraw-Hill, New York.

Leman, Gregory W., 1985. Atomization and deposition in two-phase annular flow: measurement and modelling. Ph.D. Thesis, The University of Illinois, Urbana.

Lunde, K., Nuland, S., 1997. Dispersed, stratified two-phase flow. In: Submitted to the Two-day Symposium on Annular and Dispersed Flows Organised in ExHFT4, Brussels, June.

Moody, L.F., 1944. Friction factors in pipe flow. Trans. ASME'68.

Nuland, S., Lingelem, M.N., 1993. Two-phase flow in inclined pipes at high gas density. In: 12th International Conference on Offshore Mechanics and Arctic Engineering, Glasgow.

Nuland, S., 1994. An alternative set of correlations for multiphase flow—mainly tested against dense gas data. IFE/KR/F-94/207.

Paras, S.V., Karabelas, A.J., 1991. Droplet entrainment and deposition in horizontal annular flow. Int. J. Multiphase Flow 17, 455–468.

Paras, S.V., Vlachos, N.A., Karabelas, A.J., 1994. Liquid layer characteristics in stratified-atomization flow. Int. J. Multiphase Flow 20, 939–956.

Saffman, P.G., 1965. The lift on a small sphere in a slow shear flow. J. Fluid Mech 22, 385.

Skarsvåg, K., Sunde, A.J., Thue, S., 1986. Method and apparatus for investigating two-phase flow in pipes. Patent pending, London.

Vames, J.S., Hanratty, T.J., 1988. Turbulent dispersion of droplets for air flow in a pipe. Experiments in Fluids 6, 94–104.

Wallis, G.B., 1975. The terminal speed of simple drops or bubbles in an infinite medium. Int. J. Multiphase Flow 1, 491–511.

Williams, L.R., 1990. Effect of pipe diameter on horizontal annular two-phase flow. Ph.D. Thesis, The University of Illinois, Urbana.

Williams, L.R., Dykhno, L.A., Hanratty, T.J., 1966. Droplet flux distributions and entrainment in horizontal gas–liquid flows. Int. J. Multiphase Flow 22, 1–18.